Generation and control of optical rogue waves by super-Gaussian pulses with varying steepness

LU WAN,[1] HAOZHE LI,[1] ZHIXIANG DENG,[1] YANXIA GAO,[2] DIANYUAN FAN,[1] AND LIFU ZHANG[1,*]

[1] *International Collaborative Laboratory of 2D Materials for Optoelectronic Science & Technology, Institute of Microscale Optoelectronic, Shenzhen University, Shenzhen 518060, China*
[2] *School of Physics and Optoelectronic Engineering, Shenzhen University, Shenzhen 518060, China*
[*] *zhanglifu@szu.edu.cn*

Abstract: We investigate the dynamic of optical rogue waves induced by super-Gaussian (SG) pulses in fiber optic. SG pulses with controlled steep leading and trailing edges can produce high-intensity self-focusing when propagate in nonlinear fibers with weak dispersion and strong nonlinearity. We observe the emergence of various rogue waves, including Peregrine breathers, Akhmediev breathers (AB) and 2nd-order AB. By adjusting the steepness of the SG pulses, the generation of these rogue waves can be controlled. As the steepness of the SG pulse increases, we find the fundamental-order AB can stably coexist. Simultaneously, we reveal that the period of these ABs can be effectively controlled by adjusting the steepness of the SG pulse. At a certain steepness, the 2nd-order AB with high power can also be observed. We also investigate the propagation of SG pulses with an initial chirp in fiber optic and found that they can also control AB and 2nd-order Peregrine breathers. Our findings present a new approach to generating controllable rogue waves.

1. INTRODUCTION

Rogue waves (RWs), also referred to as deformed waves or giant waves, are waves with extraordinarily large amplitudes and possess the rare and unpredictable characteristics [1–4]. In the beginning, investigations on RWs were mainly focused on the ocean [5, 6], and then there was an extensive investigation in other fields of physics, including nonlinear optics [7–9], plasmas [10] and Bose-Einstein condensates [11]. In 2007, the first observation of the existence of optical RWs was reported in the work of Solli *et al*., when they investigated the heavy-tailed histograms of intensity fluctuations in supercontinuum generation [12]. Since then, optical RWs have been attracting the interest of research on both theoretical and experimental sides, due to their potential applications and relative ease of creation and capture in laboratory settings [13]. The optical RWs have now been successfully observed in many optical settings such as optical fibers [14], mode-locked lasers [15], Raman fiber lasers [16] and photorefractive ferroelectrics [17].

Several possible physical mechanisms for the formation of RWs have been identified, such as modulation instability and nonlinear superposition or collision of several breathers [18, 19]. The focusing nonlinear Schrödinger equation (NLSE) is the simplest partial differential equation that can be used to describe the propagation of optical waves in fibers. Its modulational instability phenomenon is believed to be a fundamental mechanism for the formation of RWs [20]. The analytical solutions of the NLSE referred to as soliton on finite background or breathers have been identified [21, 22]. Among those are the Akhmediev breather (AB), the Kuznetsov-Ma breather (KM) and the Peregrine breather (PB), and they are also known as RWs solutions [23]. AB and KM are periodic in time and space, respectively, while PB is localized both in time and space. In 2010, Kibler *et al*. proved PB in nonlinear optical fiber experiments [24], and subsequent studies in different optical media and optical systems discovered the existence of PB [25–27]. The dynamics of AB and KM solitons in optical fibers have also been verified and

observed [28–31].

Pulses with different initial conditions as input to focusing NLSE are also a method to stimulate the formation of RWs. Research in the semiclassical (zero-dispersion) limit of the focusing NLSE revealed a fundamental mechanism that universally leads to the emergence of local PB [32]. Experiments using high-power pulses injected into optical fibers show the universality of PB in focusing NLSE [33]. A rectangular barrier is considered as the initial condition for focusing NLSE, it is also known as the box problem, which describes the evolution and interaction of two counter-propagating nonlinear wave trains [34]. The generation of RWs in the box problem for the focusing NLSE has been theoretically analyzed [35], and this phenomenon has also been observed in experiments involving focusing dam-break flows in single-mode fiber [36]. Topological control of RWs has been achieved both theoretically and experimentally in focusing photorefractive medium with rectangular pulses as the initial condition [37]. These experiments and theories have investigated the focusing evolution of the 12th-order super-Gaussian (SG) pulse. However, the dynamics of RWs generated by SG pulses of different steepness still require further investigation.

In this paper, we report the propagation of SG pulses with different steepness in nonlinear fiber optic with weak anomalous dispersion. We observe that SG pulse, characterized by a flat top and two steep edges, can induce the formation of various RWs during its nonlinear propagation. The steepness of the SG pulse plays a crucial role in controlling the formation of different RWs. Through numerical simulations, we discover that the time, space, and intensity of the first focus vary depending on the steepness of the input pulse. Simultaneously, when the edges are relatively flat, we observe that the first focus sometimes present a PB structure. When the edges are steeper, the collision point of the shock waves fits well with a PB shape, and we can observe a stable AB generation. Notably, the period and intensity of the AB are dependent on the steepness of the SG pulses. Furthermore, we find that SG pulse with steeper edges can also generate a 2nd-order AB. SG pulses with initial chirp can also generate AB and 2nd-order PB in fiber optic propagation.

2. THEORETICAL MODEL

The propagation of the optical pulse can be described by the one-dimensional integrable focusing NLSE shown as follows [38]:

$$i\frac{\partial\psi}{\partial\xi}+\frac{\varepsilon}{2}\frac{\partial^2\psi}{\partial\tau^2}+\frac{1}{\varepsilon}|\psi|^2\psi=0, \tag{1}$$

where $\psi(\xi,\tau)$ is the complex field envelope that varies slowly over ξ and τ, and the parameters of Eq. (1) are all dimensionless. Physically dimensionless parameter $\varepsilon=\sqrt{L_{NL}/L_D}$, where L_{NL} and L_D are the nonlinear length and the dispersion length, respectively. For the parameter used in optics, it can be written as $\varepsilon=\sqrt{|\beta_2|/\gamma P_0 T_0^2}$, where β_2 is the group velocity dispersion coefficient, γ the third-order nonlinear coefficient.

The AB solution of Eq. (1) has the following form [39]:

$$\psi(\xi,\tau)_{AB}=\psi_0\left[\frac{\cosh\left(\Omega\xi\varepsilon^{-1}-2i\varphi\right)-\cos\left(\varphi\right)\cos\left(p\tau\varepsilon^{-1}\right)}{\cosh\left(\Omega\xi\varepsilon^{-1}\right)-\cos\left(\varphi\right)\cos\left(p\tau\varepsilon^{-1}\right)}\right]\exp\left(i\psi_0^2\xi\varepsilon^{-1}\right), \tag{2}$$

where in Eq. (2):

$$p=2\sin(\varphi),\Omega=2\sin(2\varphi), \tag{3}$$

the AB solution is periodic in time with its period $T=2\pi\varepsilon/p$. The PB solution can be obtained from the AB solution by letting $p\to 0$, and it is described by the rational solution of Eq. (1) [22].

$$\psi(\xi,\tau)_{PB} = \psi_0\left[1 - \frac{4(1+2i\xi\varepsilon^{-1})}{1+4(\tau^2+\xi^2)\varepsilon^{-1}}\right]\exp\left(i\psi_0^2\xi\varepsilon^{-1}\right). \tag{4}$$

The 2nd-order AB solution can be formed by the superposition of two ABs, and we can deduce that its expression is [40]:

$$\psi_2(\xi,\tau)_{AB} = \psi_0\left[1 - \frac{G+iH}{D}\right]\exp\left(i\psi_0^2\xi\varepsilon^{-1}\right), \tag{5}$$

where Eq. (5):

$$\begin{aligned} G =& -(\omega_1^2-\omega_2^2)\left[\frac{\omega_1^2 b_2}{\omega_2}\cosh(b_1\xi\varepsilon^{-1})\cos(\omega_2\tau\varepsilon^{-1})\right] \\ &+(\omega_1^2-\omega_2^2)\left[\frac{\omega_2^2 b_1}{\omega_1}\cosh(b_2\xi\varepsilon^{-1})\cos(\omega_1\tau\varepsilon^{-1})\right. \\ &\left.+(\omega_1^2-\omega_2^2)\cosh(b_1\xi\varepsilon^{-1})\cosh(b_2\xi\varepsilon^{-1})\right], \end{aligned} \tag{6}$$

$$\begin{aligned} H =& -2(\omega_1^2-\omega_2^2)\left[\frac{b_1 b_2}{\omega_2}\sinh(b_1\xi\varepsilon^{-1})\cos(\omega_2\tau\varepsilon^{-1})\right. \\ &\left.-\frac{b_1 b_2}{\omega_1}\sinh(b_2\xi\varepsilon^{-1})\cos(\omega_1\tau\varepsilon^{-1})\right] \\ &+2(\omega_1^2-\omega_2^2)\left[b_1\sinh(b_1\xi\varepsilon^{-1})\cosh(b_2\xi\varepsilon^{-1})\right. \\ &\left.+\omega_2\sinh(b_2\xi\varepsilon^{-1})\cosh(b_1\xi\varepsilon^{-1})\right], \end{aligned} \tag{7}$$

$$\begin{aligned} D =& 2(\omega_1^2+\omega_2^2)\frac{b_1 b_2}{\omega_1\omega_2}\cos(\omega_1\tau\varepsilon^{-1})\cos(\omega_2\tau\varepsilon^{-1}) \\ &+4b_1 b_2\left[\sin(\omega_1\tau\varepsilon^{-1})\sin(\omega_2\tau\varepsilon^{-1}) + \sinh(b_1\xi\varepsilon^{-1})\sinh(b_2\xi\varepsilon^{-1})\right] \\ &-(2\omega_1^2-\omega_1^2\omega_2^2+2\omega_2^2)\cosh(b_1\xi\varepsilon^{-1})\cosh(b_2\xi\varepsilon^{-1}) \\ &-2(\omega_1^2-\omega_2^2)\left[\frac{b_1}{\omega_1}\cos(\omega_1\tau\varepsilon^{-1})\cosh(b_2\xi\varepsilon^{-1})\right. \\ &\left.-\frac{b_2}{\omega_2}\cos(\omega_2\tau\varepsilon^{-1})\cosh(b_1\xi\varepsilon^{-1})\right], \end{aligned} \tag{8}$$

where $b_1 = \omega_1\sqrt{(4-\omega_1^2)}/2$, and $b_2 = \omega_2\sqrt{(4-\omega_2^2)}/2$. In particular, a 2nd-order AB can be formed by two AB nonlinear superposition, only when the modulation frequencies obey $\omega_1/\omega_2 = 1/2$.

The maximum compression intensity of 2nd-order PB is 25 times that of the background wave, and its form is as follows [40]:

$$\psi_2(\xi,\tau)_{PB} = \psi_0\left[1 - \frac{G_2+iH_2}{D_2}\right]\exp\left(i\psi_0^2\xi\varepsilon^{-1}\right), \tag{9}$$

$$G_2 = \frac{1}{96}\left(80\xi^4+90\xi^2\tau^2+16\tau^4+72\xi^2+24\tau^2-3\right), \tag{10}$$

$$H_2 = \frac{1}{48}\xi\left(16\xi^4+32\xi^2\tau^2+16\tau^4+8\xi^2-24\tau^2-15\right), \tag{11}$$

$$D_2 = -\frac{1}{1152}\Big(64\xi^6 + 192\xi^4\tau^2 + 192\xi^2\tau^4 + 64\tau^6 \\ -432\xi^4 + 228\xi^2\tau^2 - 48\tau^4 - 396\xi^2 - 108\tau^2 - 9\Big). \tag{12}$$

The above solutions are all referred to as the exact RW solutions of the NLSE.

3. NUMERICAL RESULTS AND DISCUSSIONS

The incident SG pulse has the following form [41]:

$$\psi(0,\tau) = \exp\left[-\frac{1+iC}{2}\left(\frac{\tau}{T_0}\right)^{2m}\right], \tag{13}$$

where m is the parameter controlling the steepness of the SG pulse, and C is the initial chirp and T_0 is the pulse half-width (peak intensity of 1/e point of pulse). According to Eq. (13), the temporal waveform of the SG pulse is affected by the shape parameter m. For $m = 1$, It is a Gaussian pulse. For $m \geq 2$, The Eq. (13) is expressed as the SG pulse. The results of the numerical simulations when m takes different values of 2, 5, and 10 are shown in Fig. 1(a). It is clear that the steepness of the leading and trailing edges of the SG pulse steepens with increasing m. Moreover, The larger the m, the shorter the time it takes for the edge of the SG pulse to rise to peak power. The rise time T_r is defined as the duration during which the intensity increases from 10% to 90% of its peak value and the relationship between T_r and m can be expressed as follows [41]:

$$T_r = (\ln 9)\frac{T_0}{2m}, \tag{14}$$

which is shown in Fig. 1(b). As the m increases, T_r shows a exponential decrease.

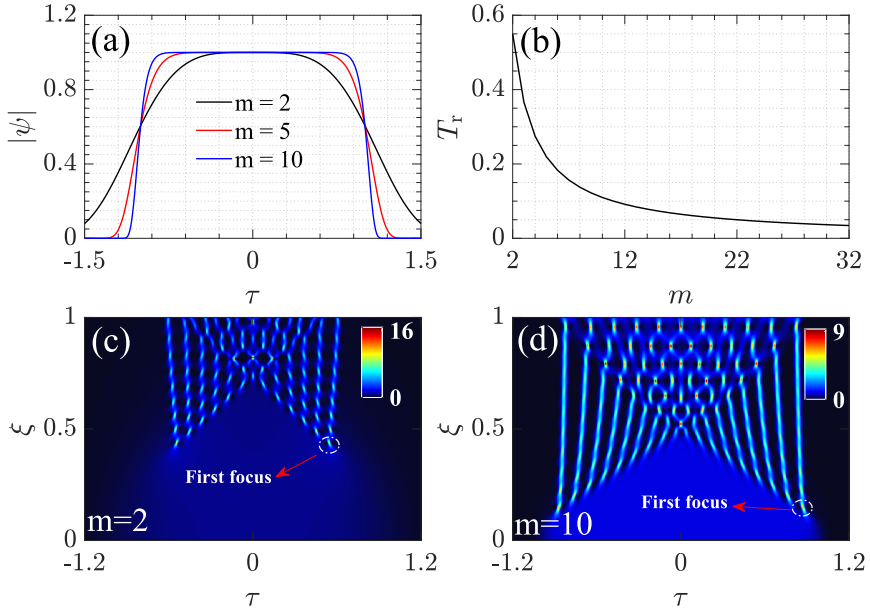

Fig. 1. (a) SG pulses with different m. (b) T_r as a function of the m. Temporal evolution of (c) $m = 2$ and (d) $m = 10$ in an anomalous dispersive, where $\varepsilon = 0.03$.

We consider the propagation of SG pulses with different initial waveforms in fiber optic, using m to change the temporal waveform of the SG pulses. In our numerical simulations, the T_0 and the dispersion parameter ε set are equal to 1 and 0.03, respectively. Figures. 1(c, d) show the temporal evolution of SG pulses with $m = 2$ and $m = 10$ in anomalous dispersion regions, respectively. As shown in the temporal evolution of SG pulse, the SG pulse will generate temporal focusing at a certain propagation distance. After the first focus, the SG pulse forms shock waves moving towards the center on both edges during propagation, and then the shock waves on both edges collide with each other [36, 37]. After shock waves collide with each other, a series of complicated breather structures are formed. It is evident that pulses of different steepness exhibit distinct compression characteristics. The distance of the first focus of a SG pulse with $m = 10$ appears closer than that of a SG pulse with $m = 2$, as shown in Figs. 1(c, d). The first focus of the SG pulse with $m = 2$ generates an RW at $\xi = 0.45$ with its intensity ~11, while the first focus of the SG pulse with $m = 10$ appears at $\xi = 0.16$ only with its intensity ~6.

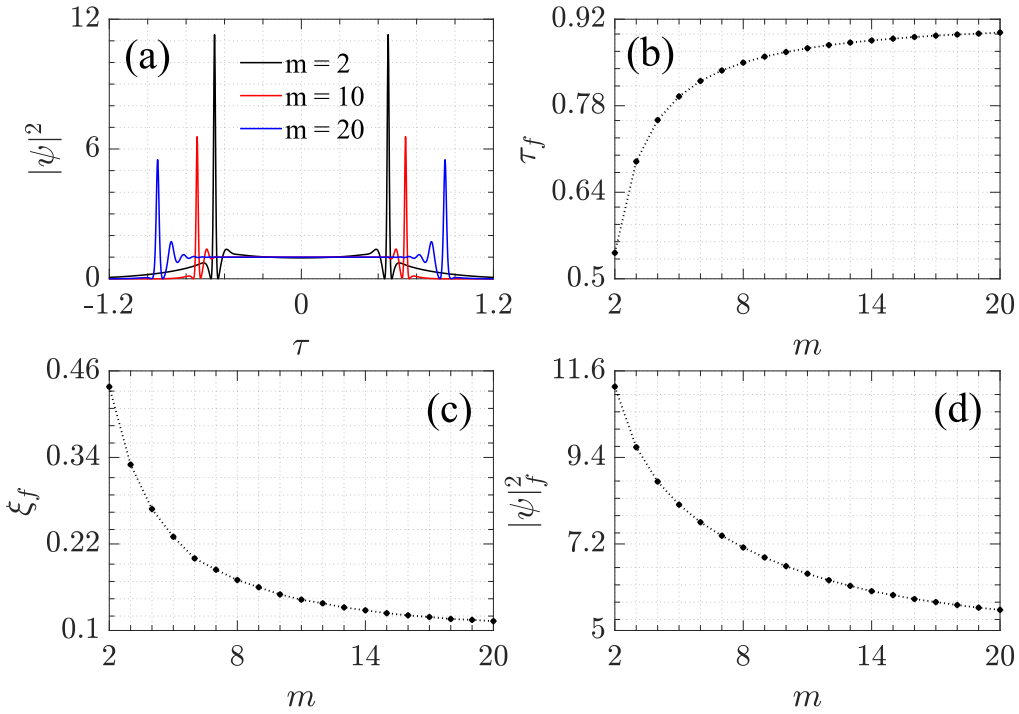

Fig. 2. (a) Temporal profiles at the first focus for evolution with different m of SG pulse input. (b-d) The time position with $\tau > 0$, distance, and peak intensity of the first focus change curves with m

We know significant differences in peak intensity ($|\psi|_f^2$), lateral time (τ_f), and distance (ξ_f) between the first focus of different m. Figure. 2(a) shows the maximum compression profile of the first focus for SG pulses with $m = 2$, 10, and 20. It is evident in the figure that the compression intensity of the first focus decreases as the m increases. To further investigate the characteristics of the first focus at different m. Figures. 2(b-d) show the variations in the time, distance, and peak intensity of the first focus on the right circled by the white solid circle in Figs. 1(c, d) with respect to m, respectively. The time increases with m, whereas the distance and peak intensity decrease exponentially with m. The propagation dynamics of different SG pulses vary due to differences in the intensity and distance of their first focus. In further propagation, the SG pulses with $m = 2$ form high-power breathers, whereas the SG pulses with $m = 20$ generate temporal

periodic breathers.

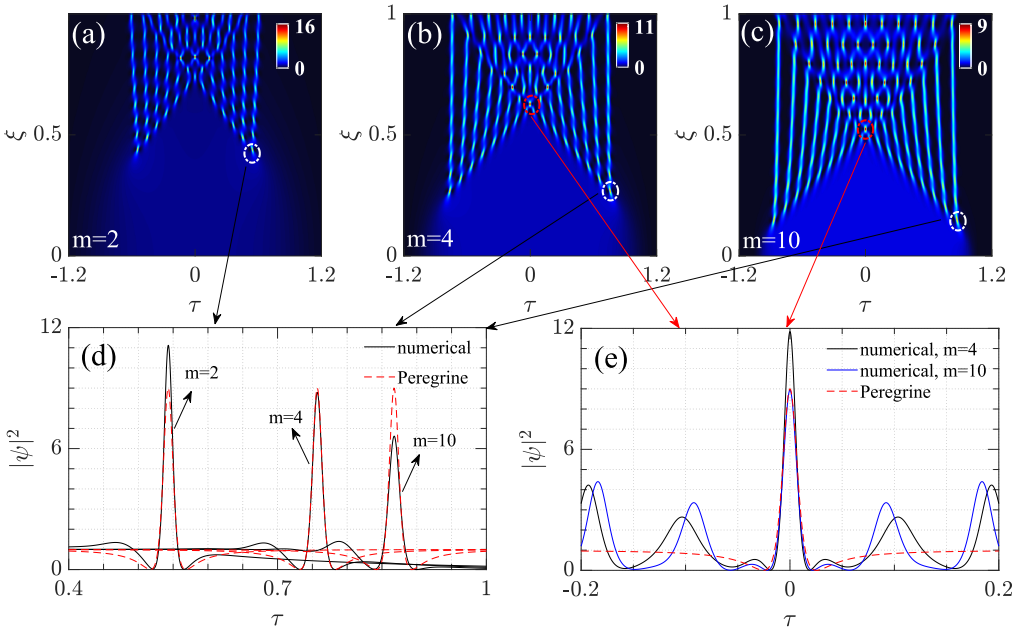

Fig. 3. (a-c) Temporal evolution of SG pulses with m values of 2, 4, and 10, respectively. (d) Comparison between the first focus and PB. (e) Comparison between collision points and PB.

When m is relatively small, the intensity of the first focus reaches the standard PB intensity, and the intensity of the collision points formed by the shock waves at both edges is also the same as the intensity of the RWs. In Figs. 3(a-c), white and red circles highlight the first focus and collision point, respectively. Figure. 3(d) shows a comparison of the intensity of PB (Eq. (4)) and the first focus of SG pulses with different m values. It can be seen from the figure that the first focus with $m = 4$ can fit well with PB, while the intensity of the first focus with $m = 2$ is slightly higher than that of the PB. Therefore, we can know that when m is small, the first focus is a RW, which degenerates into a soliton as m increases. $m = 4$ and $m = 10$ formed a high-intensity collision point at the center, and we also compare the collision point with PB, as shown in Fig. 3(e). The collision point can also fit well with PB, especially when $m = 10$. When $m = 4$, the collision point can also fit well with the PB, but the intensity is slightly higher than that of the PB.

The interaction of the shock waves results in the formation of a series of ABs during the propagation of the SG pulse with steeper edges. Figure. 4(a) illustrates the temporal evolution of an SG pulse with $m = 18$. We examined their temporal profiles at $\xi = 1$ using AB solution derived from Eq. (2). A thorough analysis of the generated AB is depicted in Fig. 4(b), revealing a remarkable agreement with Eq. (2). The temporal period T of the generated ABs can be well-controlled by m at $\xi = 1$, as shown in Fig. 4(c). Our findings demonstrate that the temporal period of the generated AB increases with m. When $m > 27$, the temporal period tends to be $T = 0.164$. Such marginal effect originates from that the steepness of SG edges is almost unchanged less with larger m. Figure. 4(a) illustrates that the peak intensity, with a temporal period, reaches a maximum value of 17 (as indicated by the color bar) at a distance of $\xi = 1.3$. Surprisingly, we find such a strong compression generates a 2nd-order AB, as shown in Fig. 4(d). The numerical simulations show good agreement with the analytical results obtained from Eq. (5) for the 2nd-order AB. It is worth noting that the 2nd-order AB is formed by the superposition of

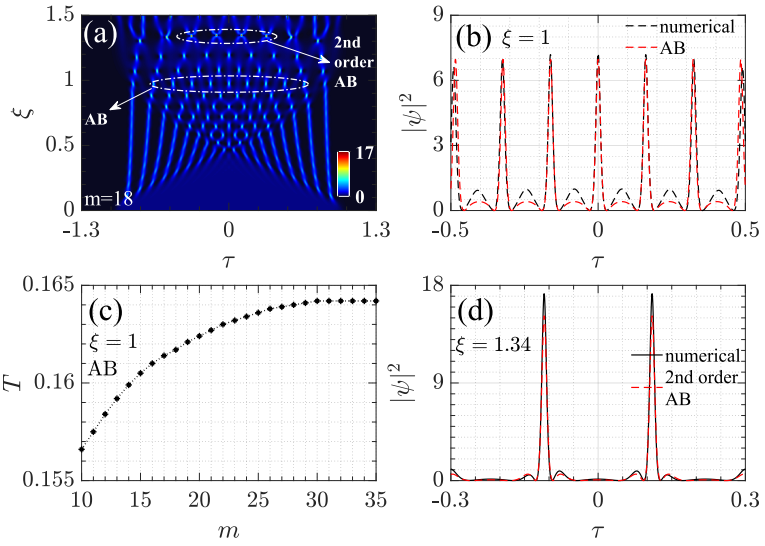

Fig. 4. (a) Temporal evolutions of the SG pulse with $m = 18$. (b) Temporal profiles of generated and analytical AB. (c) The AB period as a function of m. (d) Temporal profiles of generated and analytical 2nd-order AB.

two fundamental-order ABs, which are generated at propagation distances $\xi = 1.1$ and $\xi = 1.2$.

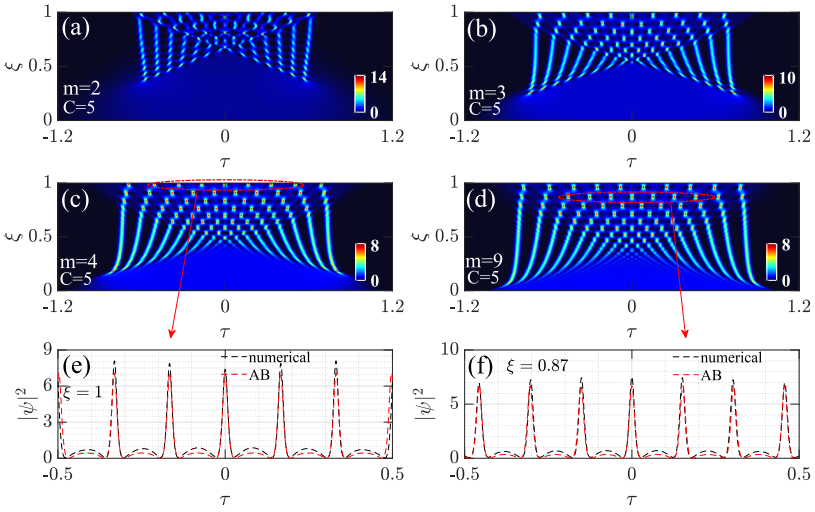

Fig. 5. (a-d) Temporal evolution of SG pulses with $m = 2$, 3, 4, and 10 under initial chirp $C = 5$. (e-f) The comparison between the breathers formed by the SG pulse with $m = 4$ and $m = 9$ at different propagation distances and the AB.

SG pulses with initial chirp can also generate RWs when propagate in fiber optic. Figures. 5(a-d) show the propagation evolution of $m = 2$, 3, 4, and 9 under initial chirp $C = 5$. From the figures, it can be seen that as m increases, the first focus disappears and both edges become twisted outward. When the initial chirp $C = 5$ and m is relatively small, the two shock waves collide with each other to form periodic breathers in time, as shown in Figs. 5(b-d). In Figs. 5(e, f), we compared the breathers of $m = 4$ and $m = 9$ with AB at propagation distances $\xi = 1$ and $\xi = 0.87$,

respectively. The comparison results show that the intensity and period can fit well with AB. In addition, when the $m = 2$ and $m = 3$, ultra-high intensity breathers will form under negative chirp, with an intensity close to 2nd-order PB. Figures. 6(a, b) show the propagation evolution of SG pulses with $m = 2$ and $m = 3$ at chirps $C = -11$ and $C = -12$, indicating the formation of a high-intensity breather during the collision of shock waves at both edges. We compare the 2nd-order PB (Eq. (9)) with the collision points and found that the intensity distribution can be well fitted, as shown in Figs. 6(c, d). The collision point intensity of $m = 2$ is higher than that of $m = 3$. When m is smaller, the intensity of the first focus is higher, and the collision point intensity formed by the interaction is also higher.

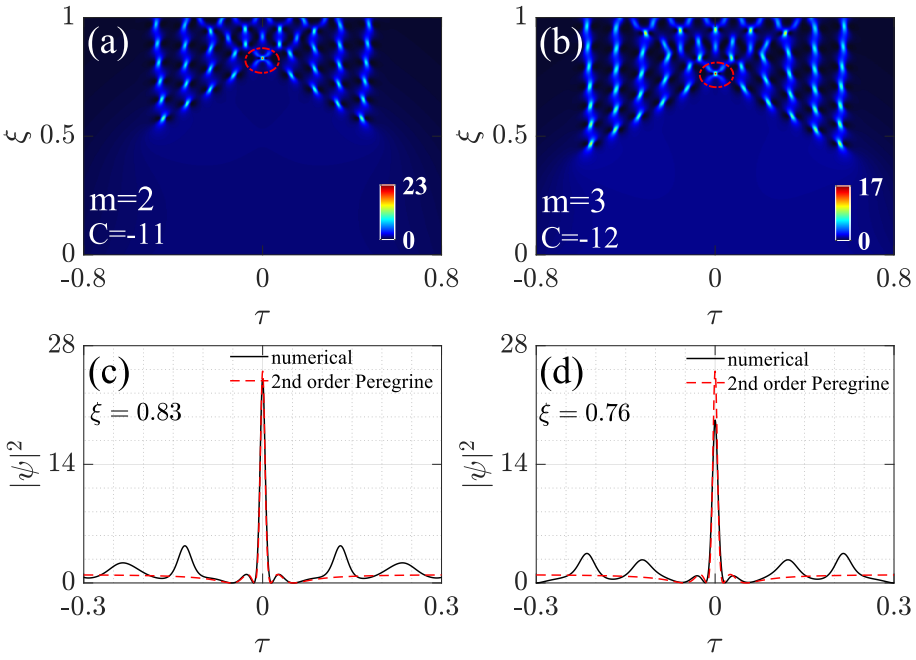

Fig. 6. (a-b) Temporal evolution of SG pulses with $m = 2$, and 3 under initial chirp $C = -11$, and $C = -12$. (c-d) The comparison of 2nd-order PB and collision points formed by SG pulses with $m = 2$ and $m = 2$, respectively.

4. CONCLUSION

In conclusion, we investigate the RWs generated by SG pulses with different steepness in fiber optic propagation. SG pulses with different steepness exhibit different propagation characteristics in fiber optic. Firstly, the intensity and distance of the first focus can be adjusted by the steepness. When m is relatively small, the first focus is RW. However, as m increases, the first focus changes from RW to a soliton. At a certain value of m, the collision point formed by the shock wave is also RW. In addition, the SG pulses with steeper edges can generate the fundamental-order ABs, of which the period can be well-controlled by the steepness of the SG pulses. The 2nd-order AB can be surprisingly generated by an SG pulse with $m = 18$. SG pulses with positive chirp can also generate AB during fiber optic propagation. Furthermore, SG pulses with negative chirp generate high-intensity 2nd-order PB during propagation. These findings will provide new inspirations for the control of RWs generation. These results demonstrate the prevalence of RWs in fiber optics and are also useful for experiments in fiber optics [36] and for wave-based computations using machine learning [42].

Funding. National Natural Science Foundation of China (61975130); Basic and Applied Basic Research Foundation of Guangdong Province (2021A1515010084).

Disclosures. The authors declare no conflicts of interest.

Data availability. Data underlying the results presented in this paper are not publicly available at this time but may be obtained from the authors upon reasonable request.

References

1. M. Tlidi and M. Taki, "Rogue waves in nonlinear optics," Adv. Opt. Photonics **14**(1), 87–147 (2022).
2. M. Närhi, B. Wetzel, C. Billet, S. Toenger, T. Sylvestre, J.-M. Merolla, R. Morandotti, F. Dias, G. Genty, and J. M. Dudley, "Real-time measurements of spontaneous breathers and rogue wave events in optical fibre modulation instability," Nat. Commun. **7**(1), 13675 (2016).
3. K. Dysthe, H. E. Krogstad, and P. Müller, "Oceanic rogue waves," Annu. Rev. Fluid Mech. **40**, 287–310 (2008).
4. T. A. Adcock and P. H. Taylor, "The physics of anomalous ('rogue') ocean waves," Reports on Prog. Phys. **77**(10), 105901 (2014).
5. N. Akhmediev, A. Ankiewicz, and M. Taki, "Waves that appear from nowhere and disappear without a trace," Phys. Lett. A **373**(6), 675–678 (2009).
6. M. Onorato, A. R. Osborne, M. Serio, and S. Bertone, "Freak waves in random oceanic sea states," Phys. Rev. Lett. **86**(25), 5831 (2001).
7. S. Chen, Y. Zhou, L. Bu, F. Baronio, J. M. Soto-Crespo, and D. Mihalache, "Super chirped rogue waves in optical fibers," Opt. Express **27**(8), 11370–11384 (2019).
8. F. Copie, S. Randoux, and P. Suret, "The physics of the one-dimensional nonlinear schrödinger equation in fiber optics: Rogue waves, modulation instability and self-focusing phenomena," Rev. Phys. **5**, 100037 (2020).
9. S. Kolpakov, S. Sergeyev, A. Udalcovs, X. Pang, O. Ozolins, R. Schatz, and S. Popov, "Optical rogue waves in coupled fiber Raman lasers," Opt. Lett. **45**(17), 4726–4729 (2020).
10. H. Bailung, S. Sharma, and Y. Nakamura, "Observation of Peregrine solitons in a multicomponent plasma with negative ions," Phys. Rev. Lett. **107**(25), 255005 (2011).
11. Y. V. Bludov, V. Konotop, and N. Akhmediev, "Vector rogue waves in binary mixtures of Bose-Einstein condensates," The Eur. Phys. J. Special Top. **185**(1), 169–180 (2010).
12. D. R. Solli, C. Ropers, P. Koonath, and B. Jalali, "Optical rogue waves," Nature **450**(7172), 1054–1057 (2007).
13. N. Akhmediev, B. Kibler, F. Baronio, M. Belić, W.-P. Zhong, Y. Zhang, W. Chang, J. M. Soto-Crespo, P. Vouzas, P. Grelu *et al.*, "Roadmap on optical rogue waves and extreme events," J. Opt. **18**(6), 063001 (2016).
14. Z. Liu, S. Zhang, and F. W. Wise, "Rogue waves in a normal-dispersion fiber laser," Opt. Lett. **40**(7), 1366–1369 (2015).
15. C. Lecaplain, P. Grelu, J. Soto-Crespo, and N. Akhmediev, "Dissipative rogue waves generated by chaotic pulse bunching in a mode-locked laser," Phys. Rev. Lett. **108**(23), 233901 (2012).
16. S. Randoux and P. Suret, "Experimental evidence of extreme value statistics in Raman fiber lasers," Opt. Lett. **37**(4), 500–502 (2012).
17. D. Pierangeli, F. Di Mei, C. Conti, A. Agranat, and E. DelRe, "Spatial rogue waves in photorefractive ferroelectrics," Phys. Rev. Lett. **115**(9), 093901 (2015).
18. S. Coulibaly, M. Taki, A. Bendahmane, G. Millot, B. Kibler, and M. G. Clerc, "Turbulence-induced rogue waves in kerr resonators," Phys. Rev. X **9**(1), 011054 (2019).
19. M. Onorato, S. Residori, U. Bortolozzo, A. Montina, and F. Arecchi, "Rogue waves and their generating mechanisms in different physical contexts," Phys. Reports **528**(2), 47–89 (2013).
20. S. Toenger, T. Godin, C. Billet, F. Dias, M. Erkintalo, G. Genty, and J. M. Dudley, "Emergent rogue wave structures and statistics in spontaneous modulation instability," Sci. Reports **5**(1), 10380 (2015).
21. N. Akhmediev, A. Ankiewicz, and J. M. Soto-Crespo, "Rogue waves and rational solutions of the nonlinear schrödinger equation," Phys. Rev. E **80**(2), 026601 (2009).
22. D. H. Peregrine, "Water waves, nonlinear schrödinger equations and their solutions," The ANZIAM J. **25**(1), 16–43 (1983).
23. B. Guo, L. Ling, and Q. Liu, "Nonlinear schrödinger equation: generalized darboux transformation and rogue wave solutions," Phys. Rev. E **85**(2), 026607 (2012).
24. B. Kibler, J. Fatome, C. Finot, G. Millot, F. Dias, G. Genty, N. Akhmediev, and J. M. Dudley, "The Peregrine soliton in nonlinear fibre optics," Nat. Phys. **6**(10), 790–795 (2010).
25. L. Bu, F. Baronio, S. Chen, and S. Trillo, "Quadratic Peregrine solitons resonantly radiating without higher-order dispersion," Opt. Lett. **47**(10), 2370–2373 (2022).
26. G. Xu, K. Hammani, A. Chabchoub, J. M. Dudley, B. Kibler, and C. Finot, "Phase evolution of Peregrine-like breathers in optics and hydrodynamics," Phys. Rev. E **99**(1), 012207 (2019).
27. F. Baronio, S. Chen, and D. Mihalache, "Two-color walking Peregrine solitary waves," Opt. Lett. **42**(18), 3514–3517 (2017).
28. B. Kibler, J. Fatome, C. Finot, G. Millot, G. Genty, B. Wetzel, N. Akhmediev, F. Dias, and J. M. Dudley, "Observation of Kuznetsov-Ma soliton dynamics in optical fibre," Sci. Reports **2**(1), 463 (2012).

29. B. Frisquet, B. Kibler, and G. Millot, "Collision of Akhmediev breathers in nonlinear fiber optics," Phys. Rev. X **3**(4), 041032 (2013).
30. J. M. Dudley, F. Dias, M. Erkintalo, and G. Genty, "Instabilities, breathers and rogue waves in optics," Nat. Photonics **8**(10), 755–764 (2014).
31. D. Pierangeli, M. Flammini, L. Zhang, G. Marcucci, A. Agranat, P. Grinevich, P. Santini, C. Conti, and E. DelRe, "Observation of fermi-pasta-ulam-tsingou recurrence and its exact dynamics," Phys. Rev. X **8**(4), 041017 (2018).
32. M. Bertola and A. Tovbis, "Universality for the focusing nonlinear schrödinger equation at the gradient catastrophe point: rational breathers and poles of the tritronquée solution to painlevé i," Commun. on Pure Appl. Math. **66**(5), 678–752 (2013).
33. A. Tikan, C. Billet, G. El, A. Tovbis, M. Bertola, T. Sylvestre, F. Gustave, S. Randoux, G. Genty, P. Suret *et al.*, "Universality of the Peregrine soliton in the focusing dynamics of the cubic nonlinear schrödinger equation," Phys. Rev. Lett. **119**(3), 033901 (2017).
34. L. Wang, Z. Yan, and B. Guo, "Numerical analysis of the hirota equation: Modulational instability, breathers, rogue waves, and interactions," Chaos: An Interdiscip. J. Nonlinear Sci. **30**(1) (2020).
35. G. A. El, E. G. Khamis, and A. Tovbis, "Dam break problem for the focusing nonlinear schrödinger equation and the generation of rogue waves," Nonlinearity **29**(9), 2798 (2016).
36. F. Audo, B. Kibler, J. Fatome, and C. Finot, "Experimental observation of the emergence of Peregrine-like events in focusing dam break flows," Opt. Lett. **43**(12), 2864–2867 (2018).
37. G. Marcucci, D. Pierangeli, A. J. Agranat, R.-K. Lee, E. DelRe, and C. Conti, "Topological control of extreme waves," Nat. Commun. **10**(1), 5090 (2019).
38. R. Jenkins and K. D. T.-R. McLaughlin, "Semiclassical limit of focusing nls for a family of square barrier initial data," Commun. on Pure Appl. Math. **67**(2), 246–320 (2014).
39. N. Akhmediev and V. Korneev, "Modulation instability and periodic solutions of the nonlinear schrödinger equation," Theor. Math. Phys. **69**(2), 1089–1093 (1986).
40. D. J. Kedziora, A. Ankiewicz, and N. Akhmediev, "Second-order nonlinear Schrödinger equation breather solutions in the degenerate and rogue wave limits," Phys. Rev. E **85**(6), 066601 (2012).
41. G. P. Agrawal, "Nonlinear fiber optics," in *Nonlinear Science at the Dawn of the 21st Century,* (Springer, 2000), pp. 195–211.
42. G. Marcucci, D. Pierangeli, and C. Conti, "Theory of neuromorphic computing by waves: machine learning by rogue waves, dispersive shocks, and solitons," Phys. Rev. Lett. **125**(9), 093901 (2020).